HHS Public Access

Author manuscript

J Mater Chem B Mater Biol Med. Author manuscript; available in PMC 2016 August 28.

Published in final edited form as:

J Mater Chem B Mater Biol Med. 2015 August 28; 3(32): 6676–6689. doi:10.1039/C5TB01319D.

Addition of Zn to the ternary Mg-Ca-Sr alloys significantly improves their antibacterial property

Guanping He[a,d,1], **Yuanhao Wu**[b,1], **Yu Zhang**[d], **Ye Zhu**[c], **Yang Liu**[e], **Nan Li**[e], **Mei Li**[d], **Guan Zheng**[a,d], **Baohua He**[f], **Qingshui Yin**[a,d,*], **Yufeng Zheng**[b,e,*], and **Chuanbin Mao**[c,*]

[a]Southern Medical University, Guangzhou 510515, China

[b]Center for Biomedical Materials and Tissue Engineering, Academy for Advanced Interdisciplinary Studies, Peking University, Beijing 100871, China

[c]Department of Chemistry and Biochemistry, Stephenson Life Sciences Research Center, University of Oklahoma, Norman, OK73019, USA

[d]Department of Orthopedics, Guangdong Key Lab of Orthopedic Technology and Implant, Guangzhou General Hospital of Guangzhou Military Command, 111 Liuhua Road, Guangzhou, Guangdong 510010, China

[e]Department of Materials Science and Engineering, College of Engineering, Peking University, Beijing 100871, China. Department of Materials Science and Engineering, College of Engineering, Peking University, Beijing 100871, China

[f]Department of Orthopedics, China Meitan General Hospital, No.29 Xibahe South street, Chaoyang District, Beijing, 100028, china

Abstract

Most of the magnesium (Mg) alloys possess excellent biocompatibility, mechanical property and biodegradability in orthopedic applications. However, these alloys may suffer from bacterial infections due to their insufficient antibacterial capability. In order to reduce the post-surgical infections, a series of biocompatible Mg–1Ca-0.5Sr-xZn (x=0, 2, 4, 6) alloys were fabricated with the addition of antibacterial Zn with variable content and evaluated in terms of their biocompatibility and antibacterial property. The *in vitro* corrosion study showed that Mg-1Ca-0.5Sr-6Zn alloys exhibited a higher hydrogen evolution volume after 100 h immersion and resulted in a higher pH value of the immersion solution. Our work indicated that Zn-containing Mg alloys exhibited good biocompatibility with high cell viability. The antibacterial studies reveal that the number of bacteria adhered on all of these Mg alloy samples diminished remarkably compared to the Ti-6Al-4V control group. We also found that the proliferation of the bacteria was inhibited by these Mg alloys extracts. Among the prepared alloys, Mg-1Ca-0.5Sr-6Zn alloy not only exhibited a strong antibacterial effect, but also promoted the proliferation of

[*]Corresponding authors: yfzheng@pku.edu.cn (YF Zheng), gz_yqs@126.com (QS Yin), cbmao@ou.edu (CB Mao).

[1]These two authors contributed equally to this work.

Electronic Supplementary Information (ESI) available: [details of any supplementary information available should be included here]. See DOI: 10.1039/x0xx00000x

MC3T3-E1 osteoblasts, suggesting that it is a promising alloy with both good antibacterial property and good biocompatibility for use as an orthopedic implant.

1. Introduction

Nowadays, the implantation of the implants into the desired place may lead to bacterial infections on the material surface or along the bone/material interface despite total disinfection prior to the surgeries.[1–4] These infections were often caused by bacteria adherence.[2, 5] After the bacterial proliferation periods, the infections associated with the implants can hardly be cured by traditional systemic antibiotic therapy due to the formation of biofilms[1]. The biofilms can also protect the bacteria against human defense system[2]. It was reported that the infection rate in orthopedic and trauma surgeries for open fracture could be up to about 1% and 12–53%, respectively.[2] Implant infections also leads to implant failure, a secondary surgery, osteomyelitis, member amputation, or even death.[1, 6–8] Although sterile operation and antibiotics were adopted in clinic situations, post-surgical infections are still one of the intractable problems.[9, 10] Hence, there is a pressing need in the development of biocompatible implants with antibacterial property.

Mg is one of the most reactive metals and, thus, susceptible to rapid dissolution, especially in chloride-containing aqueous solutions.[11] Therefore, Mg and its alloys can degrade gradually in the body fluid environment after bone healing procedure, which can eliminate the need for a second operation for implant removal.[12] The biodegradability of Mg and its alloys can also eliminate the complications associated with the long-standing presence of implants in the body and the impact on computed tomography (CT) as well as other imaging examinations. Furthermore, Mg alloys have high specific strength and a modulus that is comparable with that of human natural bones, thereby the Mg and its alloys would reduce the risk of stress shielding effect in orthopedic applications[12]. Additionally, as an essential metal element, Mg is rich in the human body and the degradation products from Mg are expected to be nontoxic to the surrounding tissue, due to the homeostatic control mechanisms.[13] Once these materials degrade within the body, the degradation products are able to be metabolized and absorbed by the body.[14, 15]

However, Mg usually exhibits a fast degradation rate before bone healing, which can lead to premature loss of the mechanical integrity and excess hydrogen evolution of the implant, resulting in the failure of the implantation[12]. Fortunately, the degradation behavior of Mg can be tailored by the alloying elements.[16–19]

Calcium (Ca) is one of the most abundant metal elements in human body, and is also the major component of human bones.[20] Meanwhile, Ca can increase the corrosion resistance of pure Mg.[17] It is reported that strontium (Sr) has the potential to stimulate bone formation[21] and Sr ranelate has shown to be effective for treating osteoporosis by increasing bone mineral density and bone strength.[22–24] Furthermore, it has been verified that adding small amount of Ca and Sr into Mg-based alloys can improve the mechanical properties of pure Mg by grain refinement mechanism.[25, 26] Berglund et al[27] further found that low amounts of alloying elements enhanced the corrosion resistance properties, with an optimal composition of 1 wt. % Ca and 0.5 wt.% Sr. The ternary alloy exhibited a higher compressive strength

than that of binary Mg-Ca alloys with similar Ca contents, and also showed negligible toxicity.

On the other hand, multifunctional biodegradable metals are in great need for biomedical applications. It is known that Zinc (Zn) is an essential mineral component for hundreds of biological enzymes and transcription factors and is widely associated with the normal function or structure of more than 300 proteins.[28, 29] Moreover, many studies[30–35] demonstrated that Zn exhibits antibacterial effect on *Staphylococcus aureus* (*S. aureus*). Thus, the addition of Zn in the Mg-Ca-Sr based alloys may produce a biomaterial with antibacterial property.

Herein, in this study, we want to combine the antibacterial property of Zn with the ternary Mg alloys (Mg-1.0Ca-0.5Sr) and fabricate the quaternary Mg-1Ca-0.5Sr-(2, 4, 6 wt.%)Zn alloys, while the Mg-1Ca-0.5Sr and Ti-6Al-4V alloys were selected as control. *S. aureus* was selected to conduct the *in vitro* antibacterial assays. The cytotoxicity of the alloys were also evaluated *in vitro* by indirect MTT assays. The antibacterial property coupled with biodegradability of the prepared Mg-Ca-Sr-Zn alloys would provide a new type of multifunctional orthopedic biomaterials.

2. Materials and methods

2.1 Preparation of magnesium alloys

Mg-Ca-Sr-Zn alloy with a nominal composition of 1 wt. % Ca, 0.5 wt.% Sr, and variable Zn (0, 2, 4, or 6 wt.%) were prepared from commercial pure Mg (99.9%), Ca (99.8%), Sr (99.9%) and Zn (99.9%). The raw Mg ingots were melt in a high purity graphite crucible under the protection of a high purity Ar (99.99%) atmosphere at about 670 °C. After the addition of the alloy elements, the temperature of the melts was increased to 720°C. After being held for about 40 min, the melts were poured into a steel mold preheated to 250°C. During the whole melting procedure, mechanical stirring was applied. The as-cast ingots of Mg-Ca-Sr-Zn alloys were solid solution treated at 340°C for about 4 h, followed by quenching in water. Finally the alloy samples were hot extruded at the temperature about 320°C with an extrusion speed of 2 mm/min. The disk sample with a diameter of 12 mm and a height of 2 mm were cut from the extruded ingots. Subsequently, the disk samples were abraded with up to 2000-grit SiC water paper and ultrasonically cleaned in acetone, absolute ethyl alcohol and deionized water for about 10min, respectively.

2.2 Microstructure characterization

X-ray diffraction analysis was applied to identify the phase composition of the alloys. For microstructure analysis, the polished alloys samples were chemically etched with a 4 vol.% nitric acid solution. The etched samples were then observed by scanning electron microscopy (SEM, Hitachi S-4800) equipped with energy dispersive spectrometry (EDS).

2.3 Immersion tests

Immersion tests were carried out in the Hank’s solution with an area/volume ratio of 1 cm^2/20 ml for about 10 days and the temperature was kept at 37 °C using water bath. During

the whole immersion periods, the pH value of the immersion solution was detected everyday using a pH meter (Sartorius, PB-10). After the indicated immersion periods, all the alloy samples were carried out of the solution and washed with distilled water for 3 times and then air dried. The surface morphology and the composition of the corrosion products on the sample surfaces were characterized by SEM (Hitachi S-4800).

2.4 Hydrogen evolution tests

A self-made set was used to determine the hydrogen evolution of the alloys in Hank's solution. Briefly, three alloy samples were soaked in the beaker containing Hank's solution with an area/volume ration of 1 cm^2/40 ml. The solution was kept at 37°C with water bath. A reversed funnel was placed over the samples, and then an acid burette filled with Hank's solution was mounted over the funnel to collect the hydrogen released from the sample surface. The hydrogen evolution volume was detected and the hydrogen evolution rate was calculated according to a reported method.[36]

2.5 Magnesium alloys extracts preparation

The extracts of Mg-Ca-Sr-Zn alloys for the antibacterial assays were prepared as follows. Before the immersion procedure, all the alloy samples were sterilized in 70% ethanol for 30 min and rinsed with a 0.85% NaCl solution. Then the alloy samples were immersed in phosphate buffered saline (PBS) solution with an extraction ratio of 1.25 cm^2/ml and incubated at 37°C in a humidified atmosphere of 5% CO_2 for 72 h, and then the extracts were centrifuged at 3000 rpm for 5 min to remove the alloys particulates, the supernatants were then collected and stored at 4°C prior to the experiments. Finally, the ion concentration of Mg, Ca Sr and Zn in the extracts were detected by Inductively Coupled Plasma Atomic Emission Spectroscopy (ICP-AES). The pH value and osmolality of the extracts were measured with pH meter (Sartorius, PB-10) and Micro-Sample Osmometer (Fiske 210), respectively. Three replicates were measured for each extract. α-MEM extracts for cytotoxicity tests were prepared in a similar way by changing the PBS solution into α-MEM medium.

2.6 Antibacterial properties

2.6.1 Bacterial culture—As one of the most common bacteria that cause orthopedic implants infections,[37] *S. aureus* (ATCC 25922) was used as a model bacterium to determine the antibacterial property of the alloys *in vitro*. *S. aureus* was aerobically cultured in a 37°C shaker incubator at 220 rpm for 16 h in 5 mL of Luria–Bertani (LB) medium containing 10 g/L peptone, 10 g/L NaCl, and 5.0 g/L beef extract. The density of the bacteria cultured in the medium was quantified by absorption spectroscopy at the wavelength about 600 nm (OD600) after performing colony counts on different concentration bacterial suspensions. OD600 was converted to colony forming units (CFU) as follows: OD600 =0.1 contained ~10^8 CFU. Serial dilution of the bacteria was performed in LB medium to achieve a final bacterial cell suspension of 1×10^6 and 1×10^7 CFU/ml, respectively.

2.6.2 Indirect bactericidal assay—For each test, 100 μl bacterial suspension and 100 μl alloys extracts were added to 800 μl PBS. The control wells contained only 100 μl bacterial suspension and 900μl PBS without the addition of alloy extracts. Microplates were then

incubated aerobically at 37 °C in a humidified atmosphere with 5% CO_2 in an incubator for 24 h. Then, aliquots of 100 μl were plated in duplicate on the agar plates. CFU were determined on the plates after incubation for another 24 h. The assays were carried out in duplicate.

In order to determine the antibacterial potency of Mg alloys with different extract time, alloy extracts were prepared by immersing the alloys in PBS for 1, 6, 12, 24, 48, 72 and 96 h with an area/volume ration of 1.25 cm^2/ml. Antibacterial curves of the alloys extracts were obtained by incubating 1 ml bacterial suspension with the extracts, which were extracted at the indicated time, for 24 h at a bacterial concentration of 10^6 CFU/ml. Then, viable bacteria were quantified by plating 100 μl of diluted aliquots in duplicate on the agar plates. CFU were determined on the plates after incubation for 24 h at 37 °C in a humidified atmosphere with 5% CO_2. The assays were carried out in duplicate.

2.6.3 Direct bactericidal assay—To evaluate the direct antibacterial property of the alloys, 1 ml of the bacterial suspension at a concentration of 10^7 CFU/ml was added to each experimental sample in 24-well plates. Then the plates were incubated at 37 °C in a humidified atmosphere with 5% CO_2 for 4 h. After the incubation procedure, the samples were gently rinsed three times with PBS in order to eliminate the non-adherent bacteria and then transferred to new tubes containing 5 ml of PBS. The samples in the tubes were then sonicated for 5 min in a 40 W ultrasonic bath at a nominal frequency of 43,000 Hz followed by vortexing for thirty seconds to remove the adherent bacteria into the PBS solutions. The viable organisms in the PBS buffers were quantified by plating serial dilutions on the LB broth agar plates. The plates were incubated for 24 h at 37 °C in a humidified atmosphere with 5% CO2, and the colony-forming units were counted with naked eyes.

To further evaluate the impact of alloys on *S. aureus* viability, live/dead staining assay was applied. Briefly, 1 ml of the bacterial suspension with a concentration of 10^7 CFU/ml *S. aureus* was added to each experimental sample in 24-well plates and then incubated at 37 °C for 30 min. The suspended and non-adhered bacteria were then gently removed by rinsing in a PBS solution. Subsequently, a LIVE/DEAD BacLight Viability Kit (Invitrogen) was used to stain the bacteria. Images of the bacteria were obtained with a fluorescence microscope (Olympus, Bx51) with a green filter (excitation/emission, 420–480nm/520–580 nm) and a red filter (excitation/emission, 480–550 nm/590–800 nm).

2.6.4 Bacterial Adhesion assay—To evaluate the anti-adherence property of the alloys, 1 ml of the bacterial suspension with a concentration of 10^7 CFU/ml *S. aureus* was added to each experimental sample in 24 well plates at 37 °C. After incubated for 4 h, the samples were taken out of the culture mediums and fixed with 3% glutaredehyde for 5 h. Then, the fixed alloy samples were rinsed in PBS three times, and each were 10 min. All the samples were then dehydrated sequentially in a series of ethanol water mixture (50%, 70%, 95% and 100%) for 10 min each, the dehydration process in 100% ethanol was repeated twice. Finally, the surfaces were air dried in a fume hood. The adhesion and spreading of the bacterial on Mg alloys and Ti-6Al-4V (control) samples were observed by SEM.

For DAPI staining, after incubated with the alloys samples for 30, 60 and 90 min, *S. aureus* was counterstained with DAPI (Roche, Germany). These immunostained bacteria were visualized under the fluorescent microscope (Olympus, Bx51) and the number of adhesion bacteria was counted in five random fields.

2.7 Proliferation and cytotoxicity tests

2.7.1 Cell culture—MC3T3-E1 pre-osteoblastic cells were adopted to evaluate the proliferation and cytotoxicity of the Mg alloys. The cells were cultured at 37°C in a humidified atmosphere of 5% CO_2 in 25-cm^2 tissue culture flasks. The cell culture medium used was modified Eagle's minimum essential medium (a-MEM, Hyclone, USA) with 4.5 g/l glucose, 10% fetal calf serum (Hyclone), 10 μg/ml ascorbic acid, 50 U/ml penicillin, and 50 U/ml streptomycin.

2.7.2 Cell viability assay—Cell proliferation testing was carried out with indirect extract assay. The cells were cultured in a 96-well tissue culture plate at a density of 2×10^4 cells/ml for 1 day to allow attachment. The medium was then replaced by 100 μl of extracts supplemented with 10% FBS. During the culture periods, the culture media were changed every two days. After incubated for 2, 4 and 6 days, the extracts were withdrawn and 200 μl of (3-(4,5-dimethylthiazol-2-yl)-2,5-diphenyltetrazolium bromide (MTT) was added to each well. After incubation for 4 h, 150 μl dimethyl sulfoxide (DMSO) was added. Optical density (OD) values from the cells in the wells were measured at 490 nm by a microplate reader (Biocell-2010, Austria). Data are presented as the mean ± standard deviation.

For the Live/Dead staining, the cells were cultured on a 24-well tissue culture plate at a density of 2×10^4 cells/ml for 1 day to allow attachment. The medium was then replaced by 500 μl of extracts supplemented with 10% FBS. The culture media were replaced every two days. After incubated in 24-well plate at 37°C in a humidified atmosphere with 5% CO_2 for 6 days, the suspended and non-adhered cells were then washed out by PBS solution. Subsequently, Live/Dead staining was applied according to the manufacturer's protocol (Sigma, USA). Briefly, 0.9 μl calcien AM and 3 μl ethidium homodimer-1 solutions were dissolved in 3 ml PBS, then 100 μl of the mixture PBS were added in each well of the 24-well plates for 30min. Then a fluorescence microscope (Eclipse Ti-S, Nikon, Düsseldorf, Germany) was utilized to observe and calculate the viability of tested cells. Viable cells show a green fluorescence through the reaction of the acetomethoxy derivate of calcein with intracellular esterase, whereas non-viable cells showed red fluorescence due to the diffusion of ethidium homodimer across damaged cell membranes and binding with nucleic acids.

2.8 Statistical analysis

The average values and standard deviation were calculated from the numerical data and plotted. Statistical analysis was conducted using the standard analysis of variance method and post-hoc analysis with the Bonferroni correction. Statistical significance was considered at $p<0.05$.

3. Results

3.1 Microstructure and phase composition

X-ray diffraction patterns of the alloys were shown in Figure 1. It indicates that the investigated alloys possess different phase compositions. In the ternary alloy, only Mg_2Ca secondary phase is detected. With the addition of different amounts of Zn, other secondary phases, including $CaZn_3$, $Ca_2Mg_5Zn_{13}$ and $Ca_2Mg_6Zn_3$, are formed. The diffraction peaks of $Ca_2Mg_6Zn_3$ phase are increasing with the further addition of Zn in the alloys.

The microstructures of the alloys observed by SEM were illustrated in Figure 2. The SEM images exhibit a typical metallographic microstructural feature. As we can see from Figure 2, the Mg-1Ca-0.5Sr ternary alloys exhibit larger grain size when compared with Zn containing alloys. The secondary phases in the alloys were mainly distributed along the grain boundaries. The Mg-1Ca-0.5Sr alloy exhibited coarser grain boundaries. In the Zn containing quaternary alloys, some round particles (indicated by the black arrows) were present in the grains. With more Zn contents in the alloys, more deposited secondary phases could be found. Figure 3 shows the chemical compositions of the secondary phases indicated by the black arrows in Figure 1 and detected by EDS analysis. Oxygen derived from the oxidation reaction during polishing and etching process was detected in all the alloys samples. The atomic percentage of the alloying elements such as Ca, Sr and Zn was increased with the increment of Zn contents.

3.2 Corrosion behavior of the alloys

The morphology of alloys after immersed in Hank's solution for 10 days is exhibited in Figure 4. All the samples are covered with a layer of corrosion products and corrosion cracks can be seen on the surface due to the dehydration procedure. The congregation of local corrosion products can be seen in the inset image of Zn containing alloys (Figure 4b,c,d). Local corrosion pit can be seen in the inset image of Mg-1Ca-0.5Sr alloys (Figure 4a). The EDS spectra were taken from the corrosion products indicated by the black arrows in Figure 4 after the materials were immersed in Hank's solution for 10 days. The results were depicted in Figure 5. Figure 5 shows that the majority of the corrosion products were composed of O and Ca elements. The alloying elements Sr and Zn, along with O, C, P elements were also detected. Zn and Sr in the corrosion products had significantly lower contents than Ca, indicating that only small amounts of Zn and Sr compounds were deposited on the sample surfaces. The EDS results suggested that the corrosion products were mainly carbonates, phosphates or oxides.

3.3 Hydrogen evolution rate and pH value of the immersion solution

The hydrogen evolution rate curves are depicted in Figure 6a. The Mg-1Ca-0.5Sr alloy exhibited a higher hydrogen release rate in the first 100 h. While for the Zn containing alloys, the hydrogen evolution rate was increased with the increasing immersion periods. However, the hydrogen evolution rate of Mg-1Ca-0.5Sr-4Zn alloy was lower than that of Mg-1Ca-0.5Sr alloy during the whole immersion periods. Moreover, for the quaternary alloys, the hydrogen evolution rate was increased during the immersion periods. Mg-1C-0.5Sr alloys suffered a faster degradation rate in the initial immersion periods. All

the pH values of the samples solution increased with the increasing immersion time (Figure 6b). After 5 days' immersion, the pH value of the samples with Zn addition became steady, while the pH value of Mg-1Ca-0.5Sr alloy solution kept increasing during the whole immersion periods. With the addition of Zn in the alloy, the pH value was a little higher than the Mg-1Ca-0.5Sr alloy.

3.4 The osmolality, pH value and ion concentration of the extracts

Figure 7 shows the osmolality and pH value detect from the extracts media. The pH value of all the extracts exhibited only a little fluctuation within 7.0 ±1.0 and there was no significant differences between the Ti-6Al-4V group and the Zn-containing group. Nevertheless, significant difference between Mg-1Ca-0.5Sr group and the Ti-6Al-4V control group was observed (Figure 7). The osmolality value of all the Mg alloy extracts did not show any significant difference in comparison to the Ti-6Al-4V control group.

The change in the ion concentration of the PBS extracts is illustrated in Figure 8. It shows higher Mg ion concentration in Zn containing alloys than in Mg-1Ca-0.5Sr group. The Zn ion concentration was different for different alloy groups with about 0.05±0.01 μg/ml for Mg-1Ca-0.5Sr-2Zn, 0.48±0.15 μg/ml for Mg-1Ca-0.5Sr-4Zn and 0.89±0.08 μg/ml for Mg-1Ca-0.5Sr-6Zn. The concentration of the Ca ion in the extracts were quite similar among all the groups. While for the Sr ions, the Mg-1Ca-0.5Sr-4Zn alloys exhibited a much higher Sr ion concentration than other groups.

3.5 Indirect bactericidal assays

In order to figure out whether the Mg alloys extracts possessed antibacterial effect or not, bacteria were incubated for 24 h in PBS extracts of experimental alloy samples. After incubation, the number of viable bacteria for all extracts from the Mg alloys samples decreased compared with that of the Ti-6Al-4V control group (Figure 9). The Zn containing alloys could achieve a killing rate of approximately 90%. However, in contrast, the number of CFUs for Mg-1Ca-0.5Sr alloy exhibited a reduction only about 28% when compared with Ti-6Al-4V control group. The inhibitory effects of all the materials on the bacterial were in such an order as Mg-1Ca-0.5Sr-6Zn<Mg-1Ca-0.5Sr-4Zn<Mg-1Ca-0.5Sr-2Zn≪Mg-1Ca-0.5Sr<Ti-6Al-4V control group. The tendency of the increased antibacterial activity with increasing Zn contents in alloys was observed and Mg-1Ca-0.5Sr-6Zn was identified as most potent antibacterial material.

3.6 Antibacterial curves

Indirect antibacterial assay suggested that all the Mg alloys extracts extracted for 72 h had antibacterial or even bactericidal activity. Then we conducted another test to evaluate the antibacterial property of the extracts derived from the alloys under different extraction time. Antibacterial curves for the *S. aureus* inoculated in Ti-6Al-4V control group or in Mg alloys groups are depicted in Figure 10. Compared to the Ti-6Al-4V control group, all the Mg alloy exhibited a slight inhibition effect on the bacterial growth after 6h extract. But there is no significant differences among the Mg alloys groups before 48 h extraction was observed. With further increasing the extraction time to 72h and 96h, the viable bacteria for the Zn-

containing alloys exhibited a sharp drop to the level where no viable bacteria could be seen on the plates. However, the viable bacteria of Mg-1Ca-0.5Sr group remained constant during the whole incubation periods. For the Zn containing quaternary alloys, the number of viable bacteria on the plates decreased with the increment of the Zn content in the alloys.

3.7 Direct bactericidal assay

In order to analyze the direct antibacterial effect of Mg alloys with different Zn content, the number of bacteria on the alloys was evaluated. The amount of adhered bacteria on all the alloy samples are illustrated in Figure 11. It can be seen that the average values for viable bacteria adhered on Mg alloys were all obviously lower than the control groups (Ti-6Al-4V). The killing rate of the Mg-1Ca-0.5Sr-4Zn and Mg-1Ca-0.5Sr-6Zn was higher than 96.6%. It was interesting to note that Mg-1Ca-0.5Sr-2Zn exhibited a relative lower killing rate of 76.9%, and meanwhile, Mg-1Ca-0.5Sr also exhibited a strong antibacterial effect with a killing rate higher than 90%, which was much higher than Mg-1Ca-0.5Sr-2Zn alloy (Figure 11f).

3.8 Bacterial Adhesion assay

The vitality of bacteria adhered on the alloy samples surfaces observed by fluorescent microscopy is displayed in Figure 12. Live bacteria were stained in green, whereas dead bacteria manifested in red. The Ti-6Al-4V alloy surface is covered with a layer of live bacteria. The results suggest that the number of live bacteria on Mg alloy samples is remarkably lower than that on Ti-6Al-4V control group. In addition, large number of dead bacteria can be seen on Mg alloy samples.

The fluorescent images of the bacterial cells stained with DAPI are shown in Figure 13 and the adhered bacteria number counted in five random fields is illustrated in Figure 14. From the Figure 13, we can find that all the alloy samples showed similar bacteria adhesion on the surfaces after 30 min of culture. When the incubation time increased to 60 min, the bacteria adhered on the alloys surfaces exhibited a decline tendency in comparison to that at 30 min (Figure 14). However, the number of bacteria attached on the Ti-6Al-4V control group was increased (Figure 14). After 90 min, the adhered bacteria on all the Mg alloy surfaces dramatically decreased, while the Ti-6Al-4V control group still showed an increase in the number of adherent bacteria (Figure 14).

SEM observation was performed to examine the morphology and number of the adhered bacteria and the results are depicted in Figure 15. It was found that the bacteria maintained their normal shape after incubation for 4 h. However, the number of bacteria on the Mg alloys surface exhibited significant decrease when compared with that of Ti-6Al-4V control group. We can conclude that Mg alloy can significantly inhibit the growth of bacteria and the adherence of the bacteria on the alloys surfaces.

3.9 Cytotoxicity

MTT assay was used to assess the cell proliferation of MC3T3-E1 cells cultured in different Mg alloys extracts for 2, 4, and 6 days. The cell viability is shown in Figure 16. It can be seen that the morphology of MC3T3 cells in different extracts was in spindle-like shape,

which was similar to that of the control group (Figure 16). As is shown in Figure 16(f), cells cultured in the Mg alloys extracts showed relatively similar absorbance in comparison to the control group on the first 2 days ($p>0.05$). Afterwards, the absorbance of all the groups was increased drastically, indicating the increase in the number of living cells. On day 4, the number of cells on the Mg-1Ca-0.5Sr group was slightly higher than that on the Ti-6Al-4V control group ($p<0.05$). Meanwhile, the number of the cells on the other three alloy groups had no statistically significant differences compared with the Ti-6Al-4V control group ($p>0.05$). After 6 days, although all the Mg alloys still exhibit a high absorbance, we can see that the cell growth rate showed a mild drop with the increase of Zn content, and the Mg-1Ca-0.5Sr group showed a statistical differences compared to the control group with an inhibition rate of about 20%.

The images of Live/Dead assay are exhibited in Figure 17. The results showed that there were a slight increase in the number of dead cells with the increase in the Zn content. The number of the dead cells on the Mg-1Ca-0.5Sr alloys were lower than the Mg-1Ca-0.5Sr-6Zn alloys after 6 days of incubation. Although a few numbers of dead cells can be seen in all the alloys extracts, the viability of the cells in Mg-Ca-Sr-Zn quaternary alloys are still higher than 80% after 6 days incubation.

4. Discussion

Bacterial infection frequently threatens the health of patients and has become the predominant causes of biomaterial implant failures.[1] Mg-Ca, Mg-Sr, Mg-Zn binary alloys have been proved to be promising orthopedic biomaterials with excellent biocompatibility and good *in vivo* behavior.[16, 17, 19] As anti-bacterial elements, both Zn and Sr were widely used in bioactive glasses for bone repairing applications. The results of this study found that our prepared Mg-Ca-Sr-Zn alloys exhibited both good anti-bacterial property and good biocompatibility.

4.1 Microstructure and *in vitro* corrosion behavior

Zn has been reported to be an efficient grain refiner for Mg alloys. In our present work, the SEM images confirmed that the addition of Zn in the Mg-1Ca-0.5Sr alloy led to the refinement of the grain size (Figure 2). The maximum solubility of the Zn in Mg is 6.2wt.% at 325°C, however, Zn containing phases including $CaZn_3$, $Ca_2Mg_5Zn_{13}$ and $Ca_2Mg_6Zn_3$ were also detected according to XRD analysis (Figure 1). It suggested that the solubility of Zn in α-Mg was decreased and the compounds were formed when other alloying elements were added. Furthermore, with higher Zn contents in the alloys, more Zn containing secondary phases were deposited in the grains or along the grain boundaries (Figure 2, 3).

Immersion test and hydrogen evolution test are two common and efficient approaches for evaluating the *in vitro* degradation behavior of the alloys for biomedical applications. After 10 days of immersion in Hank's solution, the sample surface was mainly covered with a layer of carbonates and phosphates.[17] Sr and Zn were also detected in the corrosion products (Figure 5b), indicating that the degradation of the alloys may also form Sr and Zn containing salts or oxides. Mg-1Ca-0.5Sr alloy exhibited a local corrosion mode with corrosion pits on

the surface. With the addition of Zn to the ternary alloy, no corrosion pit can be seen. The alloying element of Zn resulted in more homogenous corrosion of the alloys.

During the initial period, the hydrogen evolution rate of the Mg-1Ca-0.5Sr was higher than that of Zn-containing alloys. The fast degradation rate resulted in the higher pH value of the immersion medium (Figure 6b). With the increasing immersion time, the corrosion products deposited on the alloy acted as a protective layer and inhibited the permeation of the corrosive medium (Figure 4a). Thus, the hydrogen evolution rate decreased (Figure 6a). The released cations from the degradation process consumed the OH^- to form the deposits and pH value of the medium in Mg-1Ca-0.5Sr alloy group increased more slowly than other alloy groups (Figure 6b). With further increase in the immersion time, the corrosion product layer was broken down by the medium, and fresh alloy matrix was exposed to the medium and the hydrogen evolution rate and volume were then increased. The Zn containing alloys exhibited a slower degradation rate at the first 100 hours and Mg-1Ca-0.5Sr-4Zn alloy showed a better corrosion resistance during the whole immersion period. Moreover, Mg-1Ca-0.5Sr-6Zn alloy exhibited higher hydrogen evolution rate.

4.2 Indirect antibacterial assays

As was described in the previous sections, the bacterial colony formation numbers according to the indirect assay were decreased with the increasing Zn contents. It was widely regarded that osmolality and pH value of the culture medium were two common factors that important for the growth of cells and bacteria. Due to the buffering capacity of the PBS solution, we found that both the osmolality and pH of the PBS extracts exhibited little fluctuation between the alloys with different Zn contents, while the pH value of Mg-1Ca-0.5Sr alloy showed a statistically significant difference compared with the Ti-6Al-4V control group (Figure 7). All the osmolality and pH values of the PBS extracts were in the suitable ranges for the growth of bacteria. However, the ions concentration of the PBS extracts was different from each alloy (Figure 8). Robinson et al [6] evaluated the antibacterial properties of Mg metal *in vitro*. They found that the increment of Mg^{2+} ions released from the corrosion process alone had no anti-bacterial effect, but the increment in the pH value of the extracts inhibited the growth of bacteria. In our study, there was only little difference of the Ca^{2+} ions concentration among the four alloys, and thus we concluded that the anti-bacterial property of the Mg-Ca-Sr-Zn alloys had little correlation with the Ca^{2+} and Mg^{2+} ions. Taking this finding into consideration, the Sr^{2+} and Zn^{2+} in the PBS extractions may contribute to the anti-bacterial effect of the Mg-Ca-Sr-Zn alloys.[37] Furthermore, the number of CFUs of the Mg-Ca-Sr-Zn alloys was decreased with the increment of Zn^{2+} ion concentration (Figure 8, Figure 9), indicating that Zn^{2+} ion improved the anti-bacterial property. It was reported that the addition of Sr resulted in a dose dependent bactericidal effect in the bioactive cements.[38] An *in vivo* result also showed that the Sr-doped 45S5 bioglass didn't cause any inflammation.[39] After half or totally substituted the Ca in the hydroxyapatite (HA) with Sr, the anti-bacterial effects of HA were improved.[40] Many studies[33, 41] had demonstrated that Zn possessed excellent antibacterial ability and exhibited antibacterial effect, especially on gram-positive bacteria. Södeberg et al [42] found that gram-positive bacteria were the most susceptible bacterial group to Zn ions and much more susceptible than gram-negative aerobic bacteria. It was reported that a relatively higher

Zn ion concentration of about 1024 μg/ml showed no inhibition effect on the gram-negative aerobic bacteria, while for the gram-positive bacteria, a concentration of about 100–110 μl/ml exhibited inhibition effects. Selahattin et al [43] also found that it had an inhibition effect on *S. aureus* with a Zn concentration of about 36.4 μl/ml. Furthermore, Jin et al[29] reported that the minimum inhibition concentration of Zn ions for *S. aureus* was lower than 9 μg/ml. On the other hand, Franklin et al[44] concluded that Zn ions released from ZnO was the main reason for the antibacterial property. They found that it showed a strong inhibition effect on *S. aureus* when the concentration of Zn ion was around 10 μg/ml, which was in accordance with Jin's work[29]. In this study, the effective concentration of Zn ions from the Zn-containing Mg alloys was very low, which was about 0.05 μg/mL for Mg-1Ca-0.5Sr-2Zn, 0.48 μg/mL for Mg-1Ca-0.5Sr-4Zn and 0.89 μg/mL for Mg-1Ca-0.5Sr-6Zn. While the low Zn ion concentration in this work revealed the same inhibition effects as in the previous studies, our findings suggested that the combination of Zn ion and Sr ions exhibited better antibacterial property compared to zinc ions alone.

The results of Mg-Ca-Sr-Zn alloys extracts at different time points on bacterial growth revealed that the Zn containing alloys continuously provide anti-bacterial effects when compared with the Mg-1Ca-0.5Sr and Ti-6Al-4V control group. Moreover, the killing rate of the extracts with an extraction time of 72 h was dramatically increased (Figure 10). In order to minimize the side effects of the antibiotics and achieve the best antibacterial effect, we concluded that when these alloys were used in clinical practice, the use of topical antimicrobial agents should be gradually reduced in 72 hours after surgery.

4.3 Direct antibacterial assays

The results of direct antibacterial assays exhibited that the alloys not only inhibited the bacteria's growth but also decreased the number of the adhered bacteria on the alloys surfaces. Mg-1Ca-0.5Sr alloy exhibited a comparable antibacterial property with Mg-1Ca-0.5Sr-4Zn and Mg-1Ca-0.5Sr-6Zn alloys. The antibacterial efficiency of Mg-1Ca-0.5Sr-2Zn alloy was significantly lower than that of the other three Mg alloys. As was shown in Figure 15, after incubation with the bacteria for 6 h, the alloys surface were covered with a layer of corrosion products and corrosion cracks could also be seen. The bacteria with normal shape was adhered on the corrosion products, and the number of bacteria varies with the Zn content in the alloys. During the whole incubation periods, gas evolution immediately took place on the surface of the alloys. The resultant gas bubbles would hinder the bacterial adherence on the alloy surface. The released OH^- derived from the alloys degradation increased the local pH value, which may further have an impact on the adherence and growth of bacteria. Furthermore, the corrosion products on the sample surfaces may also play an important role on bacterial adherence. It has been reported that the corrosion products formed during the alloy degradation process contributed to bacterial death. Both Dong et al [45] and Jin et al[46] reported the antibacterial effects of $Mg(OH)_2$ and MgO. Other scholar[44] also reported that ZnO exhibited good antimicrobial efficacy. Kishen et al [47] found that the ZnO nanoparticles produced a significant reduction in the number of E. faecalis cells adhered to dentin. The increment of Zn^{2+} ions would also be an important factor that helped the anti-adherence of bacteria. We can speculate that the formation of the oxides on the surface of the samples and the rapid release of hydrogen gas and OH^- may

contribute to the anti-adherence of the bacteria on the Mg alloys (Figure 5–6). Additionally, the increase in ion concentrations (especially Zn ion) and pH values may also have an influence on the growth of bacteria. The immersion medium of Mg-1Ca-0.5Sr-2Zn alloy group exhibited a lower pH value than other three Mg alloys. While the hydrogen evolution rate of the Mg-1Ca-0.5Sr-2Zn alloy was also slower than that of the Mg-1Ca-0.5Sr-6Zn alloy. Thus the number of adhered bacteria was higher than other Mg alloys, which may be the reason for its lower direct antibacterial and anti-adherence efficiency.

The result of Live/Dead staining assay and SEM observation give us an overview of the number of the bacteria on the samples. These findings were in agreement with that of the direct antibacterial test (Figure 11f), further confirming the antibacterial effect of the Mg alloys. The DAPI staining assay used to evaluate the early anti-adhesion property of the alloys. The results indicated that all the Mg alloys could inhibit the adhesion of bacteria when compared with the Ti-6Al-4V control group (Figure 13, 14). Furthermore, the continuous corrosion process would result in the continuous release of hydrogen bubbles and OH^- near the sample surface, thus the Mg alloys can continuous inhibit the bacterial adherence while the adhered bacteria on the Ti-6Al-4V surface was increased with the increasing incubation time.

4.4 Cytotoxicity

Ca, Sr and Zn are all essential metal element for human daily metabolism. Previous studies had already shown that these alloying elements possess good biocompatibility and osteogenic activity. In our MTT assay, the Mg-Ca-Sr-Zn alloys exhibited no obvious toxicity to MC3T3 -E1 cells and the cytotoxicity of all the alloys extracts was found to be Grade 0–1 (Figure 16). We can see that the Zn-containing alloys exhibited a higher biocompatibility than Mg-1Ca-0.5Sr. The optical images showed that the cells were spread to have a spindle-like shape. Fluorescence images also depicted that the culture disk was covered with a layer of MC3T3-E1 cells, and only a small amount of dead cells were found (Figure 17). Our results indicated that these alloys are safe enough to be used as a potential biomaterial for orthopedic applications.

5. Conclusions

Our results clearly showed that zinc addition into Mg-1Ca-0.5Sr to form Mg-1Ca-0.5Sr-4Zn decreased the hydrogen evolution volume and evolution rate, while bringing no additional toxicity compared to the Mg-1Ca-0.5Sr alloy. Moreover, Mg-1Ca-0.5Sr-6Zn exhibited a stronger antibacterial effect against *S. aureus* than Mg-1Ca-0.5Sr. We can conclude that Mg-1Ca-0.5Sr-6Zn was the best choice as an ideal antibacterial biodegradable orthopedic implant material since it not only has better antibacterial effect as Mg-1Ca-0.5Sr-2Zn and Mg-1Ca-0.5Sr-4Zn but also shows a comparable efficiency on promoting the growth of osteoblasts. This study shows that Mg-1Ca-0.5Sr-6Zn is a multifunctional antibacterial biodegradable implant that can be used in bone surgery to prevent bacterial infections.

Acknowledgments

This work was financed by National Natural Science Foundation of China (Grant No.81271957), National Basic Research Program of China (Grant No.2012CB619106) and Guangdong Key Lab of Orthopedic Technology and Implant Materials Construction Grant (No. 2011233-32).

Yufeng Zheng would like to thank the financial support by the National Basic Research Program of China (973 Program) (Grant No. 2012CB619102 and 2012CB619100), National Science Fund for Distinguished Young Scholars (Grant No. 51225101), National Natural Science Foundation of China (Grant No. 51431002).

Y.Zhu. and C.B.M. would also like to thank the financial support from National Science Foundation (DMR-0847758, CMMI-1234957, CBET-0854414), National Institutes of Health (1R21EB015190), Department of Defense Peer Reviewed Medical Research Program (W81XWH-12-1-0384), Oklahoma Center for the Advancement of Science and Technology (HR14-160) and Oklahoma Center for Adult Stem Cell Research (434003).

References

1. Wang JC, Wang ZP, Guo S, Zhang JY, Song Y, Dong XM, Wang XN, Yu JH. Micropor Mesopor Mat. 2011; 146:216–222.
2. Miola M, Bruno M, Maina G, Fucale G, Lucchetta G, Verne E. Mat Sci Eng C-Mater. 2014; 43:65–75.
3. Nablo BJ, Rothrock AR, Schoenfisch MH. Biomaterials. 2005; 26:917–924. [PubMed: 15353203]
4. Mei SL, Wang HY, Wang W, Tong LP, Pan HB, Ruan CS, Ma QL, Liu MY, Yang HL, Zhang L, Cheng YC, Zhang YM, Zhao LZ, Chu PK. Biomaterials. 2014; 35:4255–4265. [PubMed: 24565524]
5. Zhou PY, Xia Y, Cheng XS, Wang PF, Xie Y, Xu SG. Biomaterials. 2014; 35:10033–10045. [PubMed: 25260421]
6. Robinson DA, Griffith RW, Shechtman D, Evans RB, Conzemius MG. Acta biomaterialia. 2010; 6:1869–1877. [PubMed: 19818422]
7. Massa MA, Covarrubias C, Bittner M, Fuentevilla IA, Capetillo P, Von Marttens A, Carvajal JC. Materials Science and Engineering: C. 2014; 45:146–153. [PubMed: 25491813]
8. Liu J, Li FB, Liu C, Wang HY, Ren BR, Yang K, Zhang EL. Mat Sci Eng C-Mater. 2014; 35:392–400.
9. Arciola CR, Alvi FI, An YH, Campoccia D, Montanaro L. Int J Artif Organs. 2005; 28:1119–1125. [PubMed: 16353118]
10. Fielding GA, Roy M, Bandyopadhyay A, Bose S. Acta biomaterialia. 2012; 8:3144–3152. [PubMed: 22487928]
11. Song G, Atrens A, St John D, Wu X, Nairn J. Corros Sci. 1997; 39:1981–2004.
12. Staiger MP, Pietak AM, Huadmai J, Dias G. Biomaterials. 2006; 27:1728–1734. [PubMed: 16246414]
13. Witte F, Kaese V, Haferkamp H, Switzer E, Meyer-Lindenberg A, Wirth CJ, Windhagen H. Biomaterials. 2005; 26:3557–3563. [PubMed: 15621246]
14. Brar HS, Platt MO, Sarntinoranont M, Martin PI, Manuel MV. Jom. 2009; 61:31–34.
15. Peeters P, Bosiers M, Verbist J, Deloose K, Heublein B. J Endovasc Ther. 2005; 12:1–5. [PubMed: 15683259]
16. Gu XN, Xie XH, Li N, Zheng YF, Qin L. Acta biomaterialia. 2012; 8:2360–2374. [PubMed: 22387336]
17. Li ZJ, Gu XN, Lou SQ, Zheng YF. Biomaterials. 2008; 29:1329–1344. [PubMed: 18191191]
18. Krause A, von der Hoh N, Bormann D, Krause C, Bach FW, Windhagen H, Meyer-Lindenberg A. J Mater Sci. 2010; 45:624–632.
19. Zhang SX, Zhang XN, Zhao CL, Li JA, Song Y, Xie CY, Tao HR, Zhang Y, He YH, Jiang Y, Bian YJ. Acta biomaterialia. 2010; 6:626–640. [PubMed: 19545650]
20. Yin P, Li NF, Lei T, Liu L, Ouyang C. J Mater Sci-Mater M. 2013; 24:1365–1373. [PubMed: 23608999]

21. Marie PJ, Garba MT, Hott M, Miravet L. Miner Electrol Metab. 1985; 11:5–13.
22. Marie PJ. Osteoporosis Int. 2005; 16:S7–S10.
23. Dahl SG, Allain P, Marie PJ, Mauras Y, Boivin G, Ammann P, Tsouderos Y, Delmas PD, Christiansen C. Bone. 2001; 28:446–453. [PubMed: 11336927]
24. Tournis S. J Musculoskelet Neuronal Interact. 2007; 7:266–267. [PubMed: 17947810]
25. Brar HS, Wong J, Manuel MV. Journal of the mechanical behavior of biomedical materials. 2012; 7:87–95. [PubMed: 22340688]
26. Lee YC, Dahle AK, StJohn DH. Metall Mater Trans A. 2000; 31:2895–2906.
27. Berglund IS, Brar HS, Dolgova N, Acharya AP, Keselowsky BG, Sarntinoranont M, Manuel MV. J Biomed Mater Res B. 2012; 100B:1524–1534.
28. Brandt EG, Hellgren M, Brinck T, Bergman T, Edholm O. Physical Chemistry Chemical Physics. 2009; 11:975–983. [PubMed: 19177216]
29. Jin GD, Cao HL, Qiao YQ, Meng FH, Zhu HQ, Liu XY. Colloid Surface B. 2014; 117:158–165.
30. Diez-Pascual AM, Xu CP, Luque R. J Mater Chem B. 2014; 2:3065–3078.
31. Wood TJ, Hurst GA, Schofield WCE, Thompson RL, Oswald G, Evans JSO, Sharples GJ, Pearson C, Petty MC, Badyal JPS. J Mater Chem. 2012; 22:3859–3867.
32. Tarushi A, Psomas G, Raptopoulou CP, Kessissoglou DP. Journal of inorganic biochemistry. 2009; 103:898–905. [PubMed: 19395041]
33. Xua JA, Ding G, Li JL, Yang SH, Fang BS, Sun HC, Zhou YM. Appl Surf Sci. 2010; 256:7540–7544.
34. Phan TN, Buckner T, Sheng J, Baldeck JD, Marquis RE. Oral Microbiol Immun. 2004; 19:31–38.
35. Applerot G, Lipovsky A, Dror R, Perkas N, Nitzan Y, Lubart R, Gedanken A. Adv Funct Mater. 2009; 19:842–852.
36. Bornapour M, Muja N, Shum-Tim P, Cerruti M, Pekguleryuz M. Acta biomaterialia. 2013; 9:5319–5330. [PubMed: 22871640]
37. Looney M, O'Shea H, Gunn L, Crowley D, Boyd D. Journal of biomaterials applications. 2013; 27:937–947. [PubMed: 22207607]
38. Brauer DS, Karpukhina N, Kedia G, Bhat A, Law RV, Radecka I, Hill RG. J R Soc Interface. 2013; 10:20120647.
39. Gorustovich AA, Steimetz T, Cabrini RL, Lopez JMP. Journal of Biomedical Materials Research Part A. 2010; 92A:232–237. [PubMed: 19172615]
40. Ravi ND, Balu R, Kumar TSS. J Am Ceram Soc. 2012; 95:2700–2708.
41. Hameed ASH, Karthikeyan C, Sasikumar S, Kumar VS, Kumaresan S, Ravi G. J Mater Chem B. 2013; 1:5950–5962.
42. Söderberg TA, Sunzel B, Holm S, Elmros T, Hallmans G, Sjöberg S. Scandinavian Journal of Plastic and Reconstructive Surgery and Hand Surgery. 1990; 24:193–197. [PubMed: 2281305]
43. Atmaca S. Turkish Journal of Medical Sciences. 1998; 28:595–598.
44. Franklin NM, Rogers NJ, Apte SC, Batley GE, Gadd GE, Casey PS. Environmental science & technology. 2007; 41:8484–8490. [PubMed: 18200883]
45. Dong CX, Cairney J, Sun QH, Maddan OL, He GH, Deng YL. J Nanopart Res. 2010; 12:2101–2109.
46. Jin T, He YP. J Nanopart Res. 2011; 13:6877–6885.
47. Kishen A, Shi ZL, Shrestha A, Neoh KG. J Endodont. 2008; 34:1515–1520.

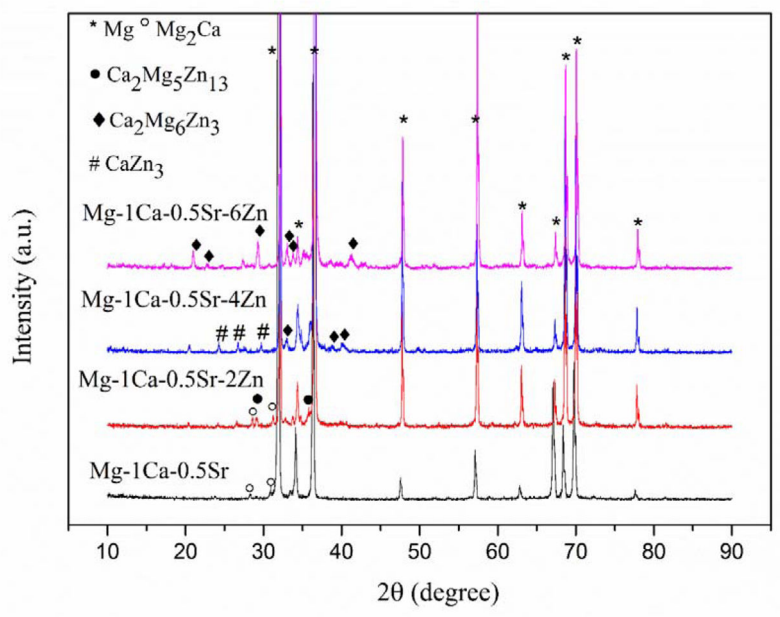

Figure 1.
X-ray diffraction patterns of the experimental alloys

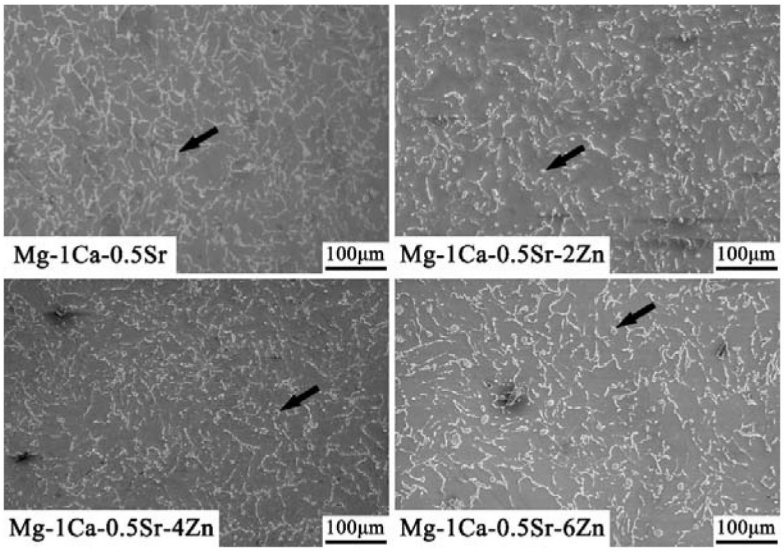

Figure 2.
The SEM images of microstructure of the Mg alloys. The secondary phases in the alloys were indicated by the black arrow.

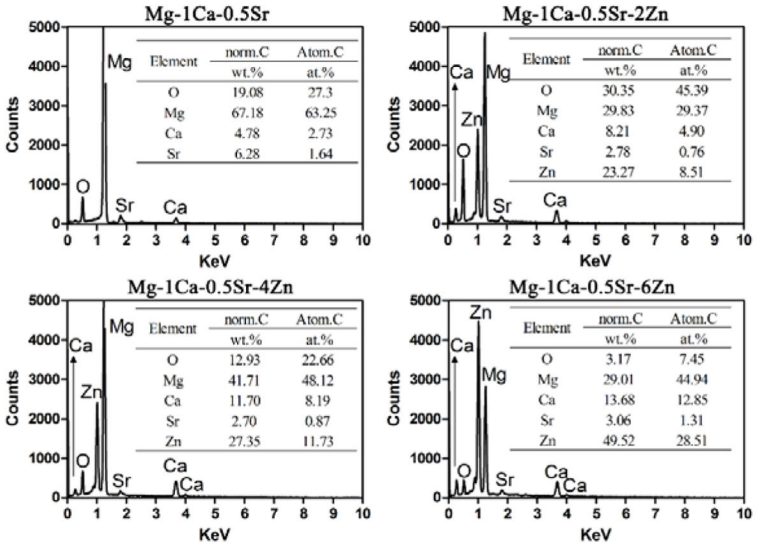

Figure 3.
EDS results of the secondary phases indicated by the arrows in Figure 2

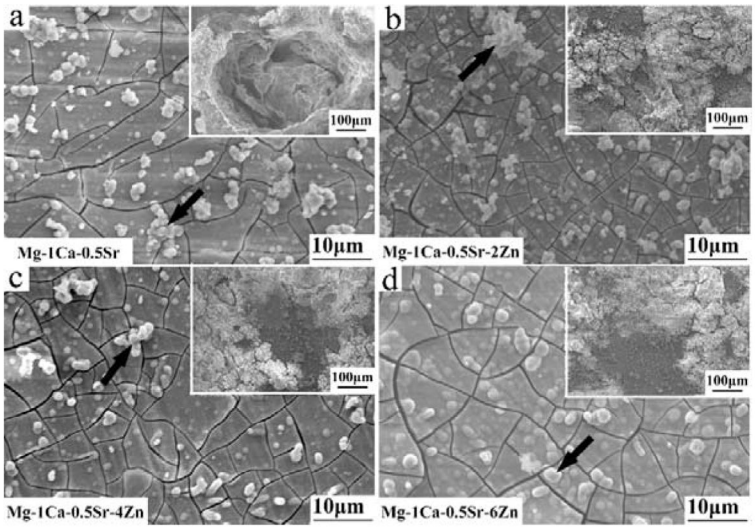

Figure 4.

Morphology of the alloys after immersed in Hank's solution for 10 days. The insets exhibited the aggregation of the corrosion products

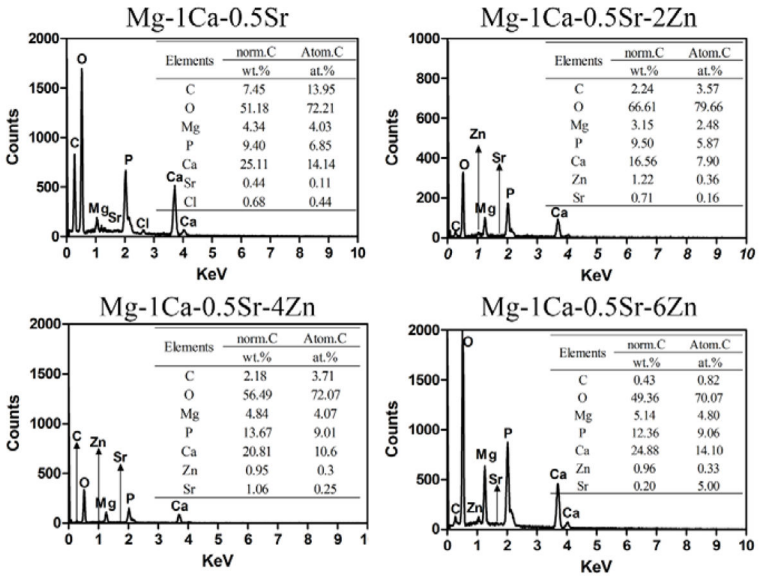

Figure 5.
EDS spectra taken from the corrosion products indicated by the black arrows in Figure 4

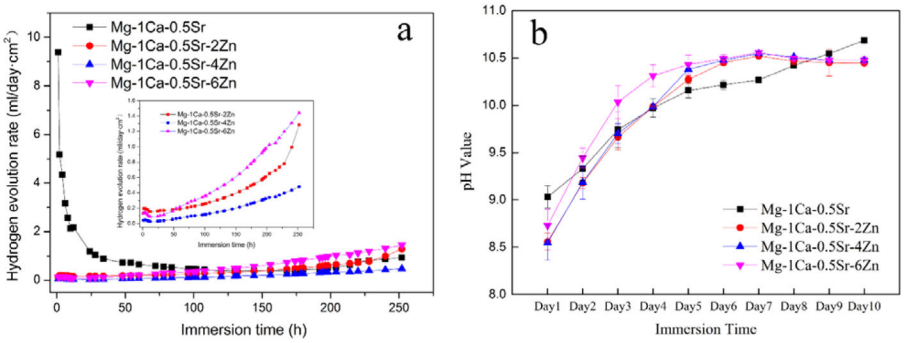

Figure 6.

Hydrogen evolution rate (a) and pH value of Hank's solution (b) as a function of immersion time. The inset picture in (a) depicts the hydrogen evolution rate of quaternary alloys.

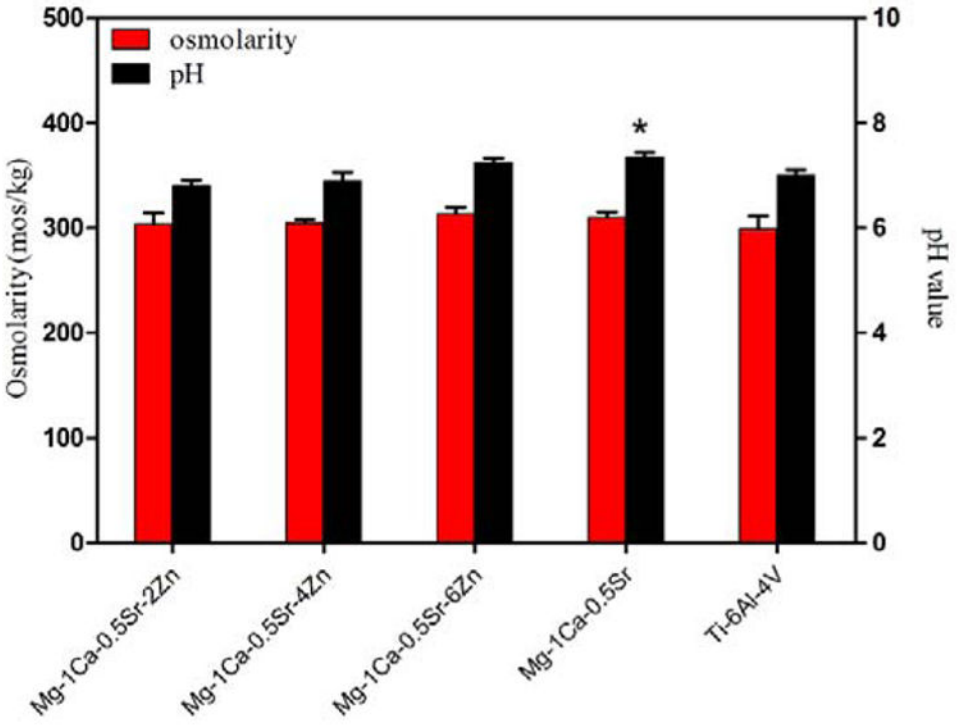

Figure 7.
Osmolarity and pH value of the PBS extracts of the alloys, * $p<0.05$

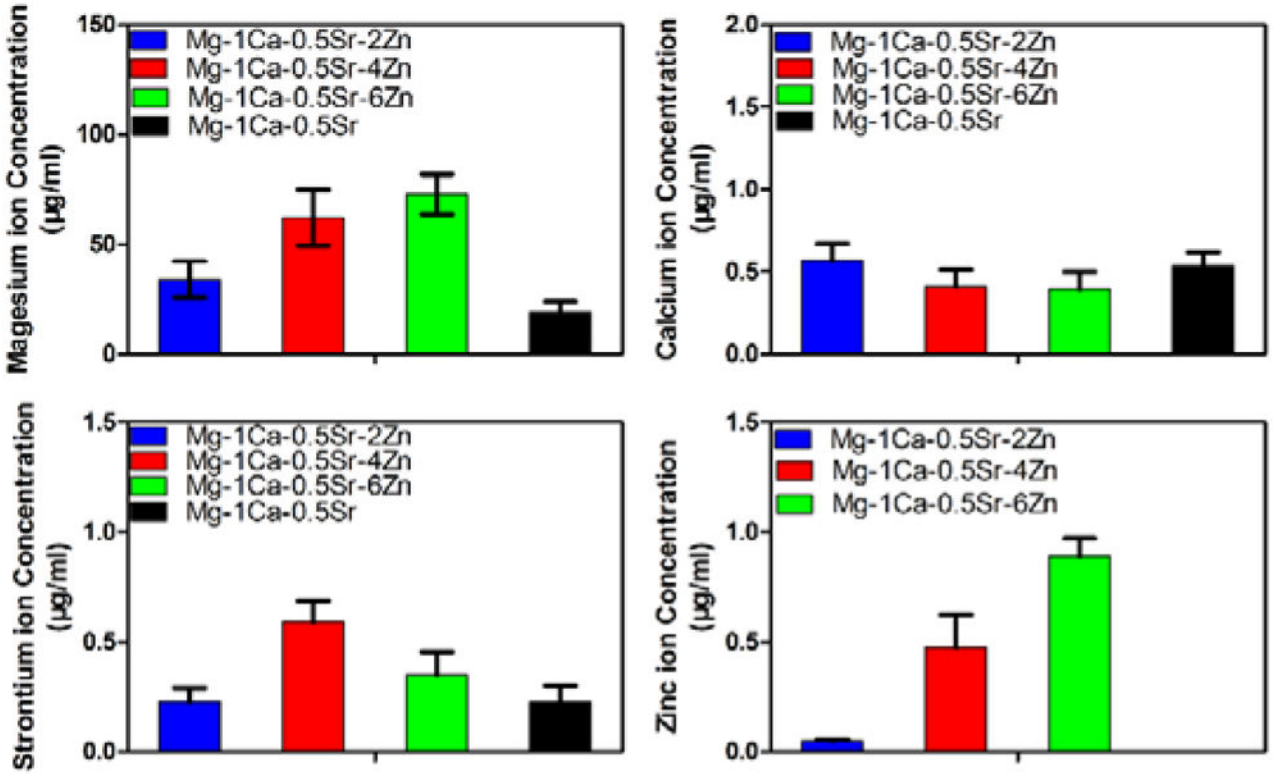

Figure 8.
Ion concentration of the PBS extracts of the alloys

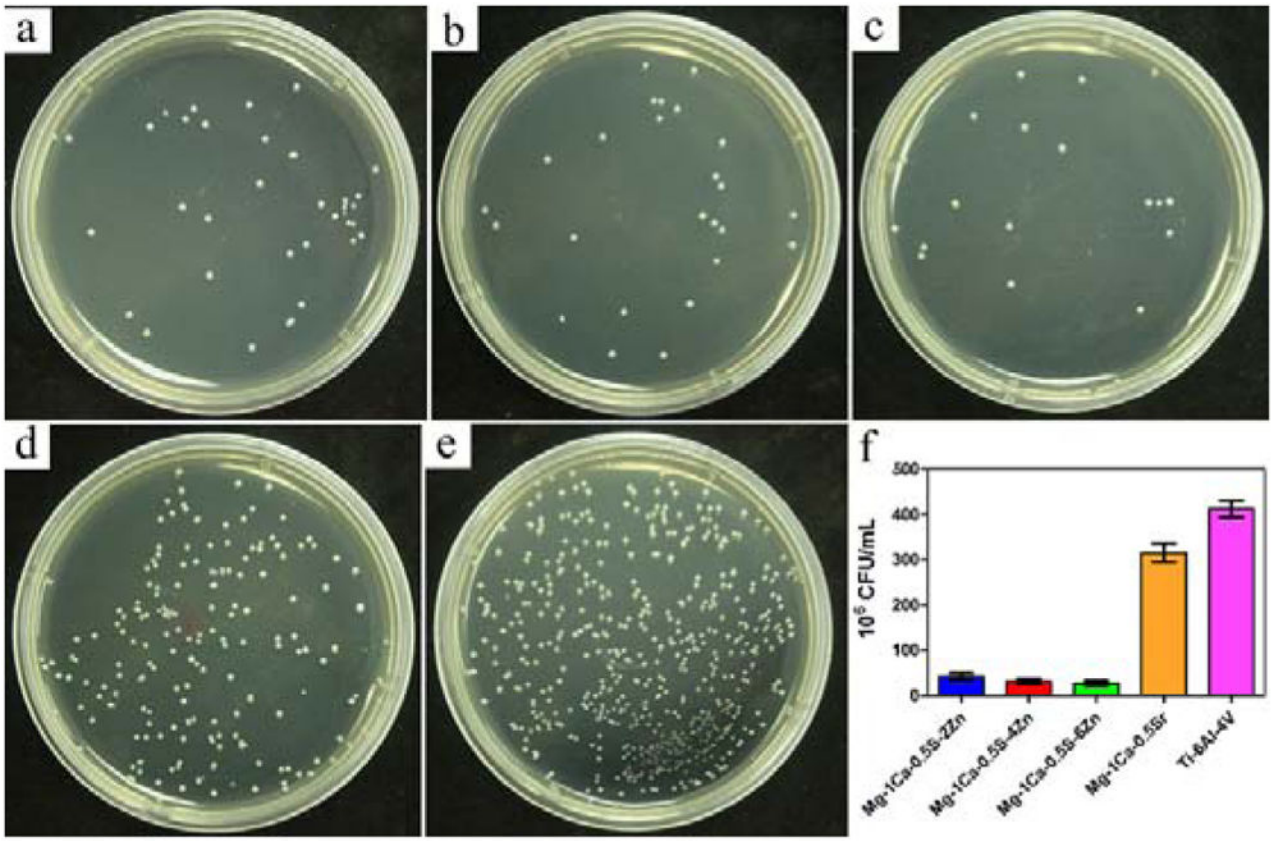

Figure 9.

S. aureus colonies after incubation with different PBS extracts of the alloys for 24 h: a) Mg-1Ca-0.5Sr-2Zn, b) Mg-1Ca-0.5Sr-4Zn, c) Mg-1Ca-0.5Sr-6Zn, d) Mg-1Ca-0.5Sr, e) Ti-6Al-4V, f) CFU of the sample alloys. The error bars represent the standard deviations calculated from three independent experiments

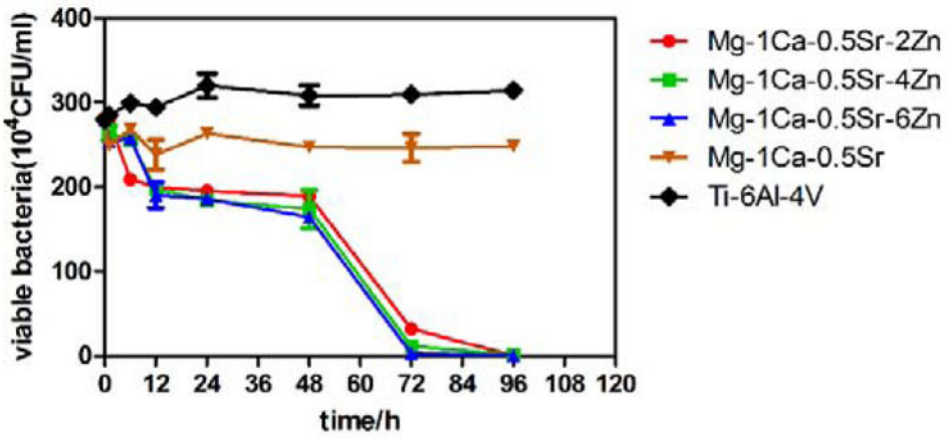

Figure 10.
Antibacterial curves of the alloys extracts extracted at different times

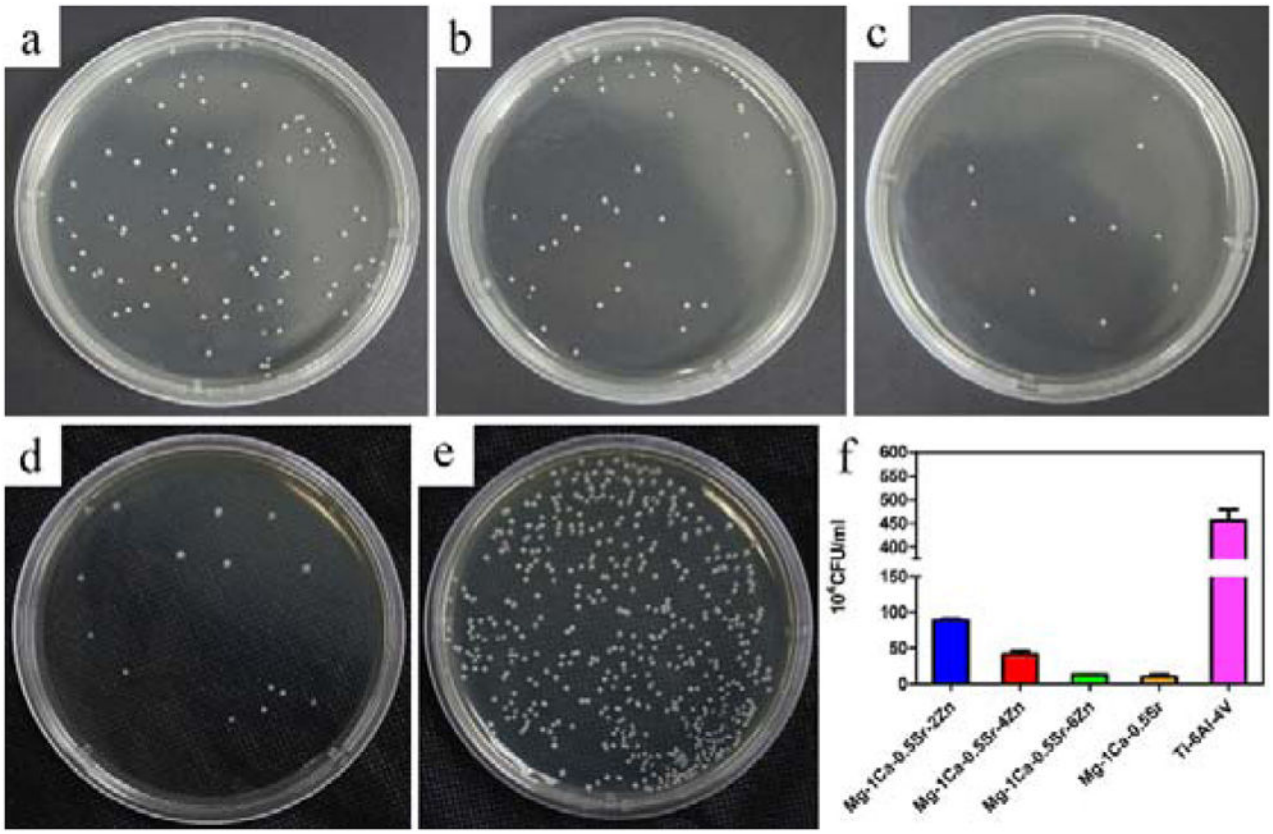

Figure 11.

S. aureus colonies incubated for 24 h after detached from the alloys surface: a) Mg-1Ca-0.5Sr-2Zn, b) Mg-1Ca-0.5Sr-4Zn, c) Mg-1Ca-0.5Sr-6Zn, d) Mg-1Ca-0.5Sr, e) Ti-6Al-4V, f) CFU of the sample alloys. The error bars represent the standard deviations calculated from three independent experiments

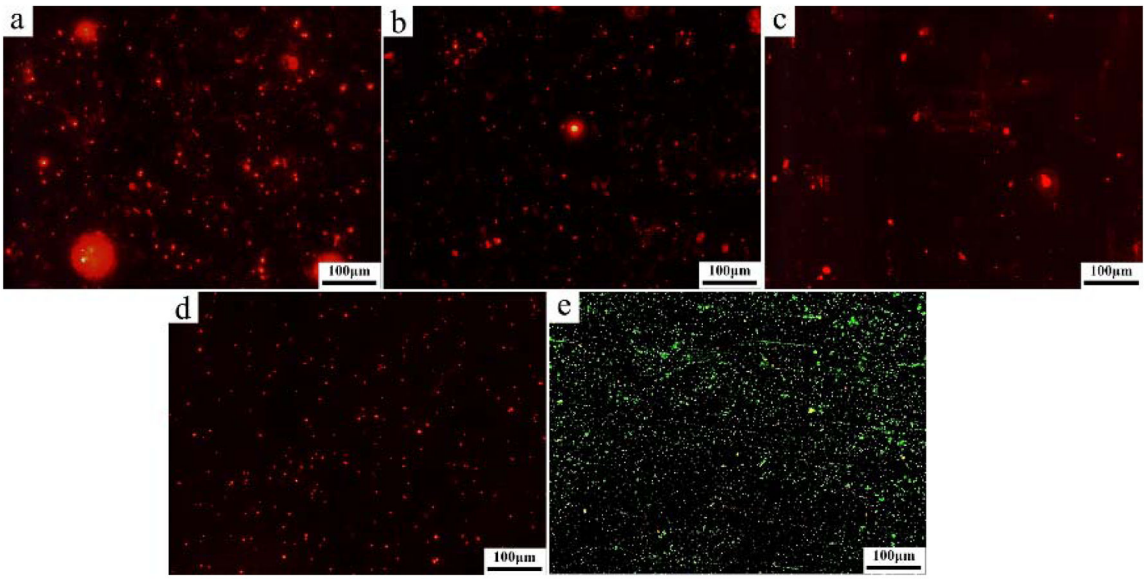

Figure 12.

Fluorescent microscopic images of *S. aureus* after 30 min of culturing on the sample surfaces: a) Mg-1Ca-0.5Sr-2Zn, b) Mg-1Ca-0.5Sr-4Zn, c) Mg-1Ca-0.5Sr-6Zn, d) Mg-1Ca-0.5Sr, e) Ti-6Al-4V. Live bacteria is in green and dead bacteria is in red

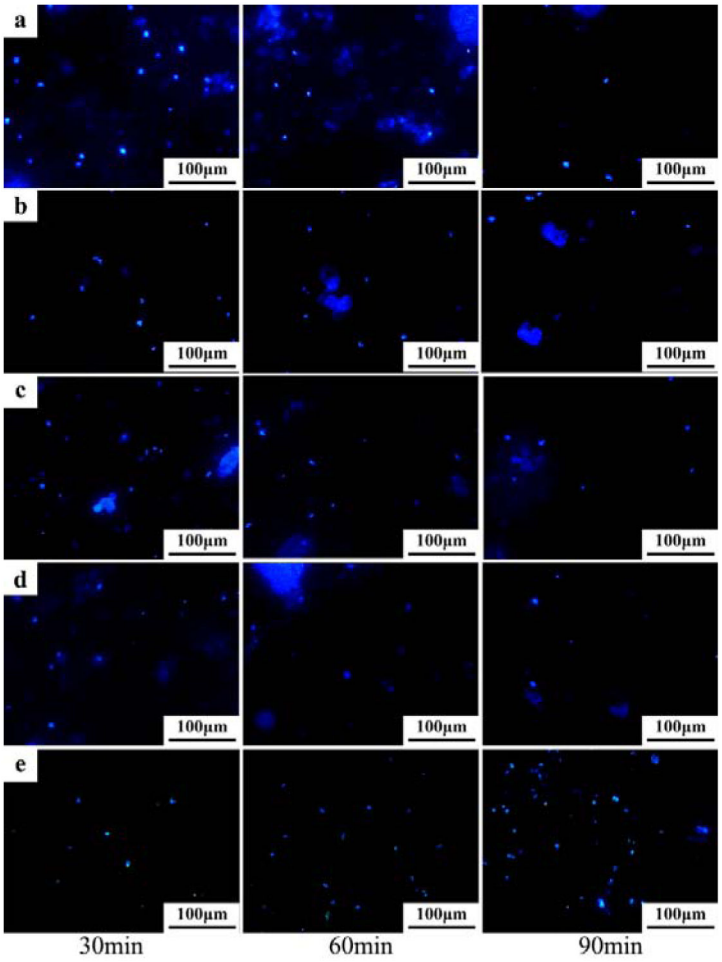

Figure 13.

DAPI staining of the adhered bacteria on the alloys surface after exposure to *S. aureus* suspension (10^7 cfu/ml) for 30 min, 60 min and 90 min: a) Mg-1Ca-0.5Sr-2Zn, b) Mg-1Ca-0.5Sr-4Zn, c) Mg-1Ca-0.5Sr-6Zn, d) Mg-1Ca-0.5Sr, e) Ti-6Al-4V

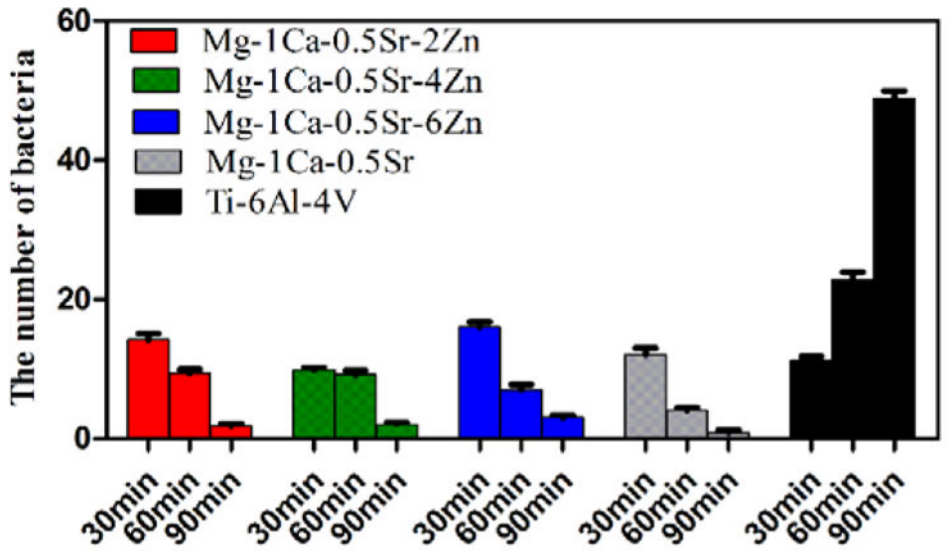

Figure 14.

The number of adhered bacteria on the alloys surfaces according to DAPI staining assay. For each alloy, five random fields were selected.

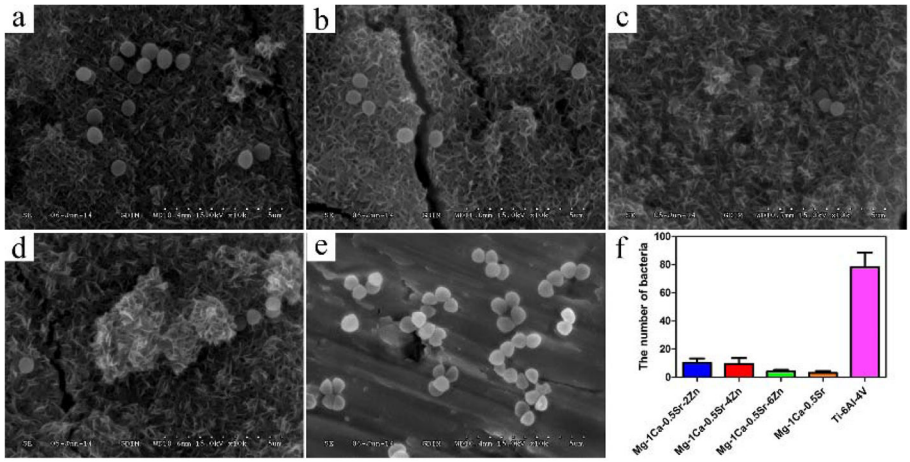

Figure 15.

SEM images of different alloys after exposure to *S. aureus* suspension for 4 h: a) g-1Ca-0.5Sr-2Zn, b) Mg-1Ca-0.5Sr-4Zn, c) Mg-1Ca-0.5Sr-6Zn, d) Mg-1Ca-0.5Sr, e) Ti-6Al-4V, f) the number of bacteria attached on the alloys surface. The error bars represent the standard deviations calculated from five independent experiments

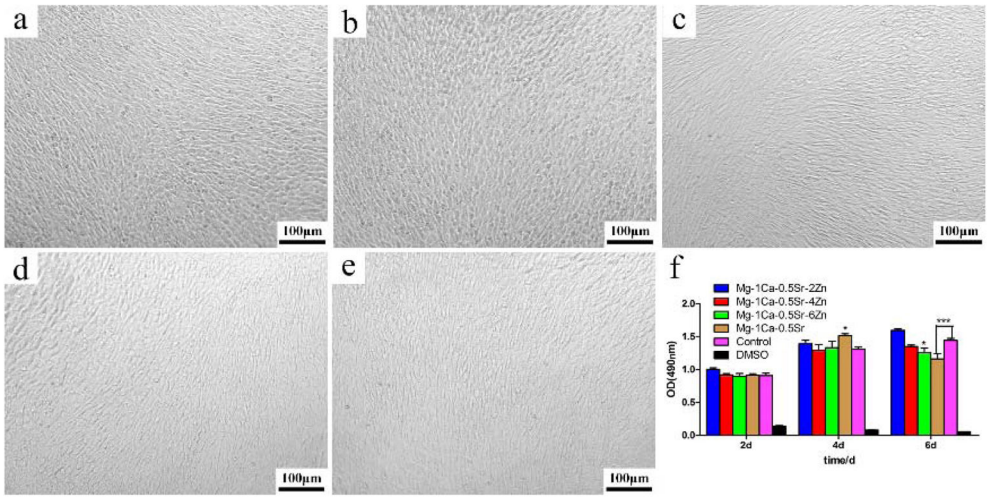

Figure 16.

Cell morphology after cultured in alloys extracts for 6 days: a) Mg-1Ca-0.5Sr-2Zn, b) Mg-1Ca-0.5Sr-4Zn, c) Mg-1Ca-0.5Sr-6Zn, d) Mg-1Ca-0.5Sr, e) Ti-6Al-4V and f) cell viability after cultured in alloys extracts for 2, 4, and 6 days. The error bars represent the standard deviations calculated from five independent experiments

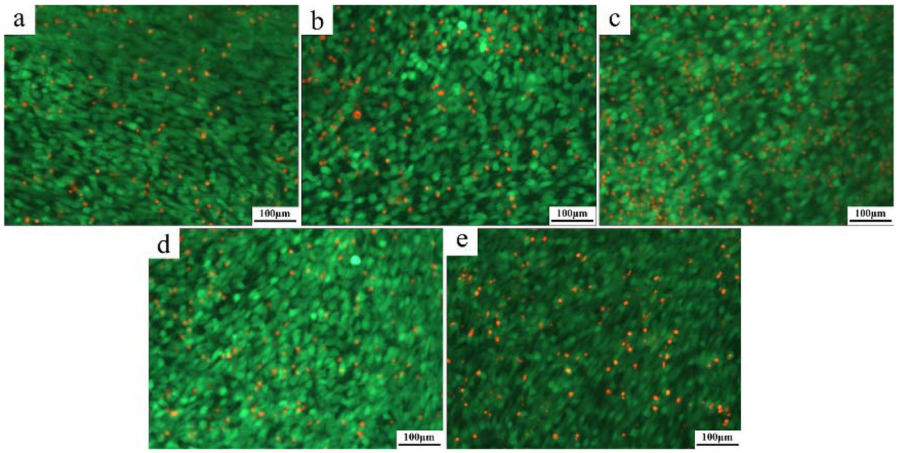

Fig. 17.

Fluorescence microscopic images of live/dead dye-stained MC3T3 cells after cultured in alloys extracts: a) Mg-1Ca-0.5Sr-2Zn, b) Mg-1Ca-0.5Sr-4Zn, c) Mg- 1Ca-0.5Sr-6Zn, d) Mg-1Ca-0.5Sr, e) Ti-6Al-4V for 6 days. Live cells are in green and dead cells are in red